

# Linking actin networks and cell membrane via a reaction-diffusion-elastic description of nonlinear filopodia initiation

Eyal Ben Isaac,<sup>1,\*</sup> Uri Manor,<sup>2</sup> Bechara Kachar,<sup>2</sup> Arik Yochelis,<sup>3,†</sup> and Nir S. Gov<sup>1,‡</sup>

<sup>1</sup>*Department of Chemical Physics, Weizmann Institute of Science, Rehovot 76100, Israel*

<sup>2</sup>*Laboratory of Cell Structure and Dynamics, National Institute on Deafness and Other Communication Disorders, National Institutes of Health, Bethesda, Maryland 20892, USA*

<sup>3</sup>*Department of Solar Energy and Environmental Physics and Ben-Gurion National Solar Energy Center, Swiss Institute for Dryland Environmental and Energy Research, Jacob Blaustein Institutes for Desert Research (BIDR), Ben-Gurion University of the Negev, Sede Boqer Campus, Midreshet Ben-Gurion 84990, Israel*

(Received 24 May 2012; revised manuscript received 8 July 2013; published 29 August 2013)

Reaction-diffusion models have been used to describe pattern formation on the cellular scale, and traditionally do not include feedback between cellular shape changes and biochemical reactions. We introduce here a distinct reaction-diffusion-elasticity approach: The reaction-diffusion part describes bistability between two actin orientations, coupled to the elastic energy of the cell membrane deformations. This coupling supports spatially localized patterns, even when such solutions do not exist in the uncoupled self-inhibited reaction-diffusion system. We apply this concept to describe the nonlinear (threshold driven) initiation mechanism of actin-based cellular protrusions and provide support by several experimental observations.

DOI: [10.1103/PhysRevE.88.022718](https://doi.org/10.1103/PhysRevE.88.022718)

PACS number(s): 87.16.A–, 82.40.Ck, 87.16.Ln, 87.16.Uv

## I. INTRODUCTION

Reaction-diffusion (RD) models are paramount in the study of pattern formation and significant to biological phenomena [1–4]. However, since reaction-diffusion models do not traditionally include the possibility of a feedback between the biochemical reactions and elastic deformations in the surrounding substrate (e.g., tissue) their validity is limited [5–7]. Recently there have been several attempts to include such a feedback in the form of RD mechanical models [8]—for example, in the context of phenomenological extension of spiral wave dynamics in cardiac tissue [9], where it was found that the elastic coupling modifies the parameter space of the RD system.

One of the intriguing frameworks of mechanical deformations pertains to the initiation and growth of actin-based protrusions, such as filopodia. These function as antennas for cells to probe their environment, and participate in a huge variety of important biological processes—cell migration [10,11], neurite outgrowth, wound healing—and serve as precursors for dendritic spine formation in neurons [12]. Due to the high complexity, various levels of different coarse graining models have been employed [13–17], but the phenomenon still remains unresolved. In this system the deformable elastic substrate is the plasma membrane of the cell, and the reactive species represent two different morphologies of cortical actin, branched and bundled, where the bundled actin emerges from the branched network due to the activity of bundle-specific nucleators [18].

Here we study the filopodia initiation by introducing a distinct model in which we couple directly between a two-state (bistable) system, which constitutes a nonlinear RD part and an elastic deformation. We exploit concepts from local and global

bifurcation theory [19] to address the problem of filopodia initiation as a generic feature. Unlike previous models [20,21], we find that the initiation of filopodia occurs as a threshold phenomenon. Previous models that treat the organization of the cortical actin in terms of RD [22,23] do not include coupling to the membrane deformation, which is the key feature in our model. We show that the coupling between the RD system and the elastic substrate supports localized states (LSs) that are *absent* in the sole RD system (under self-inhibition).

Importantly, the model is supported by experimental observations in living COS7 cells. Specifically, we find that initially extended perturbations at the membrane condense into localized filopodia structures and sometimes through merging of neighboring filopodia precursors (which individually would have decayed).

## II. REACTION-DIFFUSION-ELASTICITY APPROACH

Our model is based on the observation that the organization of the actin cytoskeleton near the cell membrane can be roughly divided into two general morphologies: The first type is a branched network of filaments that is induced by membrane proteins that activate Arp2/3 [18], while the second type is in the form of parallel actin bundles, which are typically induced by interplay between membrane proteins (e.g., IRSp53) and actin regulatory proteins (e.g., Eps8) [24] or processive actin-polymerases (such as formin [18] and VASP [25,26]), as well as actin crosslinking proteins such as fascin [27] or espin [28].

In general, these two main phenotypes involve a host of actin-binding proteins (ABPs) that are mostly active in one actin morphology but not the other. It is further observed that these two cortical actin morphologies are highly exclusive with respect to one another, although they can locally transform from one type to the other. Here we will be describing the emergence of filopodia-like protrusions in the presence of a network of branched cortical actin [29]. There are additional, independent modes of filopodia formation [30], but they are beyond the scope of this paper and will not be addressed

\*[eyalbi@weizmann.ac.il](mailto:eyalbi@weizmann.ac.il)

†[yochelis@bgu.ac.il](mailto:yochelis@bgu.ac.il)

‡[nir.gov@weizmann.ac.il](mailto:nir.gov@weizmann.ac.il)

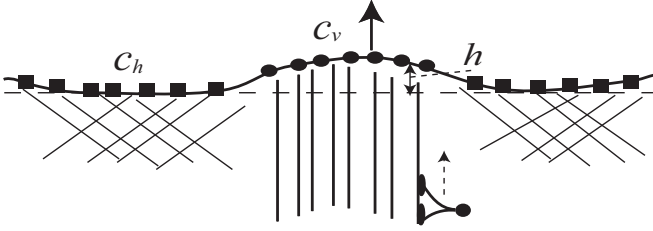


FIG. 1. An illustration of the interactions between the membranal proteins and the membrane shape, as described in the model. The squares (circles) represent the concentration of nucleators of branched (bundled) actin ( $c_h$ ,  $c_v$ ), respectively;  $h$  is the height deflection of the membrane. We illustrate a molecular motor (myosin) that carries a cargo that enhances actin bundling at the membrane. Such motors transport cargo along the bundled filaments, and not on the branched network. One example is the myosin-IIIa which transports espin cargo (actin bundling protein) to the filament tip [28].

here. Note that the two morphologies of actin may become intertwined in more complex situations, as observed for example in the formation of branched lamellipodia from the sides of bundled filopodia [31].

The reaction-diffusion-elasticity (RDE) approach, consists of an RD part of two distinct actin orientations  $c_v$  (vertical) and  $c_h$  (horizontal) and a local deformation field  $h$  (Fig. 1). The *physical* aspect of  $h$  is related to the elastic deformation that modifies the flow field of the reactive species. The system of equations used here are continuous and coarse grained. Nevertheless, the spatial resolution is sufficient to describe the local actin concentration and the membrane shape, on length scales that are smaller than the filopodia width. We additionally assume hydrodynamical fluxes, both in the actin network and in the membrane, to decay over a short range due to the dense cortical actin network. Indeed, when the membrane is detached from the actin network, such as during “blebbing” [32], hydrodynamic flow and osmotic pressure effects should be considered. The hydrodynamic flow around the membrane, and therefore issues concerning permeation, are also not treated explicitly in our model. The motion of the membrane is dominated by the dynamics of the actin cytoskeleton, and the cytoskeleton also confines the hydrodynamic flows inside the cell. We are therefore treating the surrounding fluid as providing an effective friction coefficient, which is identified with the inverse of the Oseen factor [20,21].

Motivated by the application to the filopodia initiation problem, we consider that  $c_v$  represents the concentration of membrane-bound complexes that nucleate bundled actin filaments, while  $c_h$  represents the concentration of membrane-bound complexes that nucleate branched Arp2/3-driven actin filaments. A scheme of the model is presented in Fig. 1.

We consider that the bundled actin ( $c_v$ ) induces membrane deformations, due to the protrusive force of actin polymerization. Given previous experimental [33] and theoretical [34] observations, we assume a minimal form for the coupling to the membrane deformation, where the effective membrane tension is locally *increased* due to adsorption of the branched network ( $c_h$ ). On the other hand, bundled actin ( $c_v$ ) may have enhanced binding to the membrane due to either actin-membrane linking proteins (e.g., ERM family proteins [35]) or molecular motors. These will effectively promote further the interaction between

bundled actin ( $c_v$ ) and the membrane, thus lowering the effective membrane tension.

The assumptions on which the model will be constructed are summarized as following:

(1) Two types of cortical actin morphologies are considered, characterized by both mutual-exclusion between them and by self-inhibition (decay and degradation processes).

(2) The bundled actin morphology obeys a positive feedback (self-enhancement) and exerts a protrusive force that deforms the membrane.

(3) The membrane and the actin networks are intimately connected and directly impact the dynamics of each other.

(4) Hydrodynamic flows, outside and inside the membrane, are not considered since the dense cortical actin network breaks such flows into confined domains, thus providing an effective friction.

### A. Model equations

We describe the membrane elastic energy using the Helfrich Hamiltonian [36]

$$E = \int [\Omega h^2 + (\sigma + \sigma' c_h + \sigma'' c_v)(\nabla h)^2 + \kappa(\nabla^2 h)^2] d^2r, \quad (1)$$

where  $\kappa$  is the curvature elastic modulus and  $\sigma$  is the effective membrane tension coefficient. The coupling between the membrane and the branched actin network is maintained at the linear approximation in the concentrations  $c_h, c_v$ , with coefficients  $\sigma', \sigma''$ . Thus, the attachment between the branched (bundled) network and the membrane increases (decreases) the local effective membrane tension  $\sigma' \geq 0$  ( $\sigma'' \leq 0$ ). We also add a restoring springlike term, with coefficient  $\Omega$ , to prevent any global translation of the membrane.

Minimizing the elastic energy  $E$  [Eq. (1)] for the coupling interaction between the membrane to  $c_h, c_v$ , and relating it to the membranal proteins dynamics, results in equations of motion for the protein membrane system. Similarly, variation with respect to the membrane shape gives the forces in the equation of motion for the membrane height deformation  $h$ . Altogether, the RDE model equations read as

$$\frac{\partial c_v}{\partial t} = k_{\text{on}}^v c_v - k_{\text{off}}^v c_v^3 - k_{\text{off}}^h c_h + k_{\text{on}}^{vb} C_{vb} + D_v \nabla^2 c_v + D_v \nabla \cdot \left( c_v \nabla \frac{\delta E}{\delta c_v} \right), \quad (2a)$$

$$\frac{\partial c_h}{\partial t} = -k_{\text{off}}^v c_v - k_{\text{off}}^h c_h + k_{\text{on}}^{hb} C_{hb} + D_h \nabla^2 c_h + D_h \nabla \cdot \left( c_h \nabla \frac{\delta E}{\delta c_h} \right), \quad (2b)$$

$$\frac{\partial h}{\partial t} = F_A c_v + \frac{1}{\gamma} \left( -\frac{\delta E}{\delta h} \right). \quad (2c)$$

In (2),  $\gamma$  is the local Oseen parameter (inverse of the friction) and  $F_A$  refers to the actin polymerization force. The coupling between the membrane and the actin nucleators introduces terms involving  $c_h, c_v$  in the equation for  $h$ , and involving  $h$  in the equations for  $c_h$  and  $c_v$ . The terms containing  $C_{vb}$  and  $C_{hb}$  describe the adsorption of new nucleators from the bulk of the cell cytoplasm onto the membrane. The cytoplasmic reservoir

is assumed to be very large and therefore treated as of constant density. The terms  $k_{\text{on/off}}^j$  correspond to rate constants for the binding/unbinding (on/off) reactions, while  $D_h$  and  $D_v$  are diffusion constants. The protrusive force of the bundled actin is assumed to be linearly proportional to  $c_v$  in Eq. (2c) (higher powers do not change qualitatively our results).

Next, we define dimensionless scalings:

$$\begin{aligned} c'_v &\rightarrow \beta c_v, & \beta &= \sqrt{\frac{k_{\text{on}}^v}{k_{\text{off}}^v}}, \\ c'_h &\rightarrow \alpha c_h, & \alpha &= \frac{k_{\text{on}}^v}{k_{\text{off}}^h} \sqrt{\frac{k_{\text{on}}^v}{k_{\text{off}}^v}}, \\ t' &\rightarrow T t, & T &= \frac{1}{k_{\text{on}}^v}, \\ h' &\rightarrow \tilde{h} h, & \tilde{h} &= \frac{F_A}{\gamma \sqrt{k_{\text{on}}^v k_{\text{off}}^v}}, \\ x' &\rightarrow \lambda x, & \lambda &= \sqrt{\frac{D_v}{k_{\text{on}}^v}}, \end{aligned}$$

and

$$\begin{aligned} C_p &= \frac{\sigma' D_h}{D_v^2 k_{\text{off}}^v} \left( \frac{F_A}{\gamma} \right)^2, & C'_p &= \frac{\sigma''}{D_v k_{\text{off}}^v} \left( \frac{F_A}{\gamma} \right)^2, \\ S_{h1} &= \frac{\sigma}{D_v \gamma}, & S_{h2} &= \frac{\sigma' k_{\text{on}}^v}{D_v \gamma k_{\text{off}}^h} \sqrt{\frac{k_{\text{on}}^v}{k_{\text{off}}^v}}, \\ S_{v2} &= \frac{\sigma''}{D_v \gamma} \sqrt{\frac{k_{\text{on}}^v}{k_{\text{off}}^v}}, & \tilde{\kappa} &= \frac{\kappa k_{\text{on}}^v}{D_v^2 \gamma}, \tilde{\Omega} = \frac{\Omega}{k_{\text{on}}^v \gamma}, \\ a_1 &= \frac{(k_{\text{off}}^h)^2 k_{\text{off}}^v}{k_{\text{off}}^v k_{\text{on}}^v}, & D &= \frac{D_h}{D_v}, \varepsilon = \frac{k_{\text{off}}^v k_{\text{on}}^v}{k_{\text{off}}^h k_{\text{off}}^v}, \\ a_0 &= \frac{k_{\text{off}}^h k_{\text{off}}^v}{k_{\text{off}}^v k_{\text{on}}^v} \left( \frac{k_{\text{on}}^h C_{hb}}{k_{\text{on}}^v} - \frac{k_{\text{off}}^h k_{\text{on}}^h C_{vb}}{(k_{\text{on}}^v)^2} \right), \end{aligned}$$

by which Eqs. (2) become dimensionless (dropping the apostrophe from now onwards):

$$\frac{\partial c_v}{\partial t} = -c_h + c_v - c_v^3 + \nabla^2 c_v - \nabla \cdot J_{c_v}(h) \quad (3a)$$

$$\frac{\partial c_h}{\partial t} = \varepsilon(-c_v - a_1 c_h + a_0) + D \nabla^2 c_h - \nabla \cdot J_{c_h}(h) \quad (3b)$$

$$\frac{\partial h}{\partial t} = c_v - F_{\text{elastic}}, \quad (3c)$$

where the positive parameters  $a_1$  and  $a_0$  determine the reaction kinetics and control how many homogeneous steady states are available,  $\varepsilon \geq 0$  is the time-scale ratio between the two fields,  $D$  the diffusion coefficient ratio. The membrane shape induces additional currents of the branched and bundled actin respectively  $J_{c_h}(h)$ ,  $J_{c_v}(h)$ , and an elastic restoring force acting

on the membrane  $F_{\text{elastic}}$ :

$$J_{c_h}(h) = -C_p [c_h \nabla (\nabla h)^2] / 2, \quad (3d)$$

$$J_{c_v}(h) = -C'_p [c_v \nabla (\nabla h)^2] / 2, \quad (3e)$$

$$\begin{aligned} F_{\text{elastic}} &= \tilde{\Omega} h - \tilde{\kappa} \nabla^4 h + S_{h1} \nabla^2 h + S_{h2} \nabla \cdot (c_h \nabla h) \\ &\quad + S_{v2} \nabla \cdot (c_v \nabla h). \end{aligned} \quad (3f)$$

## B. Biological and physical correspondences

The first term in Eqs. (3a) and (3b) describes the mutual exclusivity of the two actin morphologies, and we elaborate here on possible biological mechanisms behind this phenomenon. In biological terms, the inhibition between the two types of actin nucleators at the membrane can be through chemical signaling. Alternatively, mutually exclusive activities for some actin-binding proteins such as Eps8 can also be represented by this model of inhibition; Eps8 can participate in either crosslinking (e.g., bundling) or capping (e.g., branched network formation) activity, depending on whether it is bound to IRSp53 [24] or Abi1 [37], respectively [38]. Another realization of the mutual inhibition between the two actin morphologies is in the form of the competition between WASP and VASP at the leading edge of cells [39]: (i) VASP produces bundled actin filaments at the filopodia tips and also acts as an antibranching factor [12]; (ii) bundled filaments can become decorated by side branches due to the activity of WASP (together with Arp2/3), and therefore lose their ability to self-enhance the bundled phase by motor transport (see below). In this manner each type of nucleator naturally expels the other type, and this is expressed quantitatively in Eqs. (3a) and (3b).

It is observed that the branched actin network induces a rather uniform force on the membrane, which forms a background upon which the filopodia formation occurs. We therefore do not consider the direct contribution of the branched network to the actin force that pushes the membrane [Eq. (3c)]. To simplify the analysis we furthermore assume that the branched actin ( $c_h$ ) described in Eq. (3b) has only simple (linear) adsorption and decay terms. The self-inhibition term,  $a_1 > 0$ , may arise from simple steric hindrance and a linear degradation (decay) process. The inhibition term due to  $c_v$  can also arise from simple steric expulsion.

The second and third terms in Eq. (3a) for the bundled actin ( $c_v$ ) give rise to a bistable system, which is a key property that arises in our model. Bistability is obtained by solving the coupled algebraic equation for the homogeneous (uniform) states:

$$-c_h + c_v - c_v^3 = 0, \quad (4a)$$

$$-c_v - a_1 c_h + a_0 = 0. \quad (4b)$$

Note that these equations are decoupled from the membrane deformations. When the nullclines intersect at three points, each on a different branch of the cubic nullcline Eq. (4a), the system is bistable. Each one of the two fixed points in the outer regions represent stable uniform solutions while the fixed point in the inner region is unstable to small uniform perturbations [2].

Consequently, solutions to Eqs. (4) manifest two observed stable states of actin morphologies, bundled or branched: The stable solutions are either rich in  $c_h$  and poor in  $c_v$ , or vice versa. The self-enhancement [second term in Eq. (3a)] is

balanced by a high-order inhibition [third term in Eq. (3a)]. These terms in the equation for  $c_v$  describe a system that has a region of coexistence (similar to a Ginzburg-Landau treatment of an aggregating system; see Appendix). In the context of the cell, we view these terms as phenomenologically describing various self-enhancement and inhibition processes that are unique to the bundled morphology. One prominent mechanism for self-enhancement that is unique to the bundled actin is the active transport of proteins by myosin molecular motors (Fig. 1). An illustration of this mechanism is given by the activity of myosin-X in promoting filopodia formation [40]. It is postulated that myosin-X can directly induce the bundling of actin filaments at the membrane directly through its motor activity. In addition, myosin-X is known to be a carrier of VASP, which acts as a “processive capper” and induces actin bundle formation. Finally, myosin-X was found to selectively walk on bundled (as opposed to branched) actin [41]. Altogether, this system provides a natural manifestation of the self-enhancement property of the bundled actin  $c_v$  in our model.

Another example for such a process is the transport by myosin-IIIa molecular motors of espin cargo proteins along bundled actin filaments, and the observation that this myosin: cargo complex boosts the elongation of these filaments [28]. The espin cargo proteins are known to interact with actin filaments and promote bundling at the barbed ends, which are near the cell membrane. Each one of the filaments in the bundle is able to recruit additional motor: cargo pairs [8] at a constant rate (determined by the cytoplasmic myosin-IIIa: cargo concentration), giving rise to the linear self-enhancement term in Eq. (3a). Furthermore, while espin is not endogenously expressed in these cells, myosin-IIIa may itself induce bundling of actin filaments [42].

For the nonlinear self-inhibition process, one example is the auto-phosphorylation reaction between myosin-IIIa motors which causes their inactivation [43], although this does not apply to our experiments since the construction we are using does not contain the kinase domain involved in auto-phosphorylation. Another and a more general example of cooperative self-inhibition is the phenomenon of “traffic jams” of motors, as observed for myosin-X in filopodia [44]. A sufficient degree of cooperativity in the self-inhibition process would lead to a term with a high power of  $c_v$  in Eq. (3a). Note that any power equal or higher than 3 gives a system with multiple uniform steady states, and we therefore chose the lowest power to describe this self-inhibition phenomenon that still makes the system bistable. Another source of self-inhibition is the effect of excluded volume, which results in a  $-c_v^2$  term in Eq. (3a). Such a term can be included, but since bistability can be achieved without it, we chose for simplicity to ignore it.

### III. THRESHOLD PHENOMENA

The main effect of coupling between the membrane shape deformations and the cortical actin (RDE model) can be summarized as following: Since the branched network increases the local tension, in order to minimize the elastic energy there is an additional current [ $J_{c_h}(h)$  in Eq. (3d)] which transports the nucleators of the branched network ( $c_h$ ) away

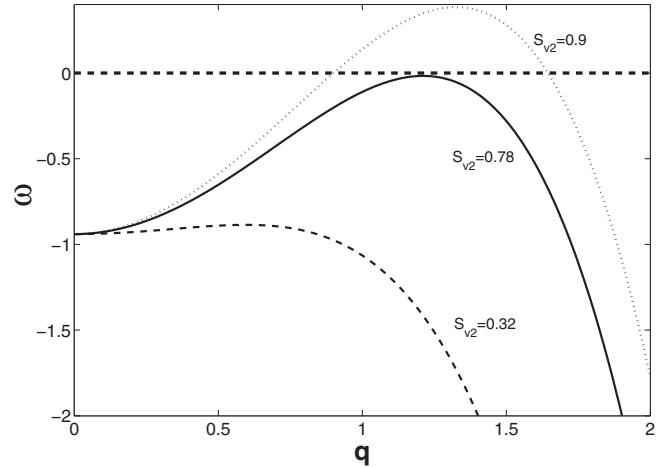


FIG. 2. Dispersion relations showing the linear instability of a uniform state to finite wave number perturbations. Parameters are given in Table I.

from regions with large gradients in the membrane shape. This flux therefore expels the branched network from the region of membrane protrusions and thus may trigger nonlinear effects. Next, we analyze the model equations.

#### A. Linear analysis to nonuniform perturbations

First, we chose a regime in which the two uniform states are stable to small nonuniform perturbations. The stability is deduced via linearization, i.e., taking weak spatially periodic perturbations for the three fields  $c_v, c_h, h$  about the uniform state (fixed point):

$$X \rightarrow X^* + \delta X e^{\omega t + i q x} + \text{c.c.} + O(\delta X^2), \quad (5)$$

where  $X^*$  is the uniform state value for the three fields,  $\delta X$  is an infinitely small perturbation,  $\omega$  is the perturbation growth rate,  $q > 0$  is the wavenumber, and c.c. stands for complex conjugate. The value of the uniform state of the fields  $c_v^*, c_h^*$  is given by the solutions of Eqs. (4), and for the membrane shape  $h^* = 0$ .

Inserting Eq. (5) into Eqs. (3) yields in the leading (linear) order

$$\omega \delta c_v = \delta c_v - 3c_v^{*2} \delta c_v - \delta c_h - q^2 \delta c_v, \quad (6)$$

TABLE I. Parameter values for Eqs. (3) that were used in calculations (unless stated otherwise).

$C_p$	0.047
$C'_p$	0
$S_{h1}$	0.537
$S_{h2}$	0
$S_{v2}$	0
$\tilde{\kappa}$	0.1
$\tilde{\Omega}$	0.28
$D$	0.0001
$\varepsilon$	0.2
$a_0$	2.72
$a_1$	1.794

$$\omega \delta c_h = -\varepsilon \delta c_v - \varepsilon a_1 \delta c_h - Dq^2 \delta c_h, \quad (7)$$

$$\omega \delta h = \delta c_v - (\tilde{\Omega} + \tilde{k}q^4 + S_{h1}q^2 + S_{h2}c_h^*q^2 - S_{v2}c_v^*q^2)\delta h. \quad (8)$$

$$\omega \begin{pmatrix} \delta c_v \\ \delta c_h \\ \delta h \end{pmatrix} = \begin{pmatrix} 1 - 3c_v^{*2} - q^2 & -1 & 0 \\ -\varepsilon & -\varepsilon a_1 - Dq^2 & 0 \\ 1 & 0 & -\tilde{\Omega} - \tilde{k}q^4 - S_{h1}q^2 - S_{h2}c_h^*q^2 + S_{v2}c_v^*q^2 \end{pmatrix} \begin{pmatrix} \delta c_v \\ \delta c_h \\ \delta h \end{pmatrix}. \quad (9)$$

Solving for  $\omega$  ( $\omega$  is real), we obtain three dispersion relations among which two have ultimately negative growth rates,  $\omega < 0$  for all  $q$ , and one which exhibits for a critical  $S_{v2} \approx 0.78$ , a finite wave number instability, as numerically shown in Fig. 2.

### B. Nonlinear behavior and spatially localized states

After determining the stability range, numerical solutions of Eqs. (3) show that the coupling between actin dynamics and membrane elasticity allows the model to support LSs, in a wide range of parameters. Throughout the paper we use (unless stated otherwise) parameters that are given in Table I while LS persists also for finite values of  $C'_p$  and  $S_{v2}$  (as demonstrated in Fig. 3). Notably, under self-inhibition (which is inherent in our physical system), Eqs. (3a) and (3b) should not support a stable LS [Fig. 4(a)], unlike other similar models, such as the well-known FitzHugh-Nagumo model [45,46], for which  $a_1 < 0$ . Detailed bifurcation analysis is beyond the scope of this study and will be addressed elsewhere.

For coupled equations, stable LSs are found in the regime where the branched network is dominant, and would have fully expelled any bundled actin in the absence of the actin-membrane coupling. We find an existence of a core of bundled actin ( $c_v$ ) which is “protected” from the inhibitory effects of the branched network ( $c_h$ ) by the deformation of the membrane and the resulting expulsion of the branched network. The LS shape is stable to small perturbations, since opposing forces

From the above we can determine the stability of the uniform solutions, i.e., calculating the growth rate ( $\omega$ ) by taking a determinant of the stability matrix:

maintain its finite width: A small increase in width of both the membrane protrusion and distribution of  $c_v$  results in lower gradients of the membrane shape, and therefore a lower expulsion flux of  $c_h$  [ $J_{c_h}(h)$ , Eq. (3d)]. The branched network

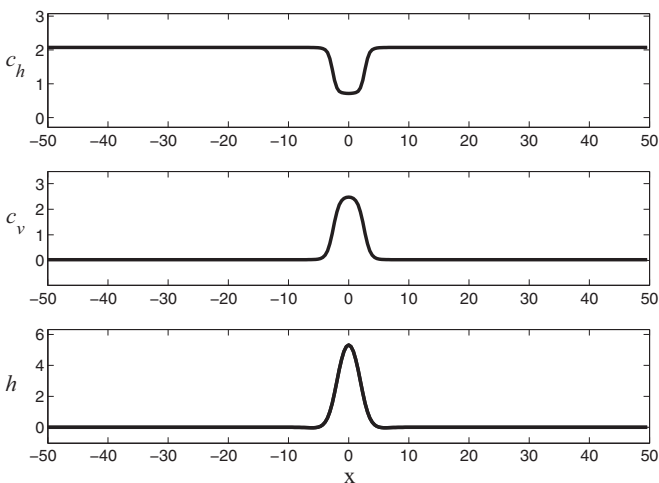


FIG. 3. Asymptotic localized solution for  $S_{v2} = 0.32$  and  $C'_p = 0.005$  while other parameters as in Table I.

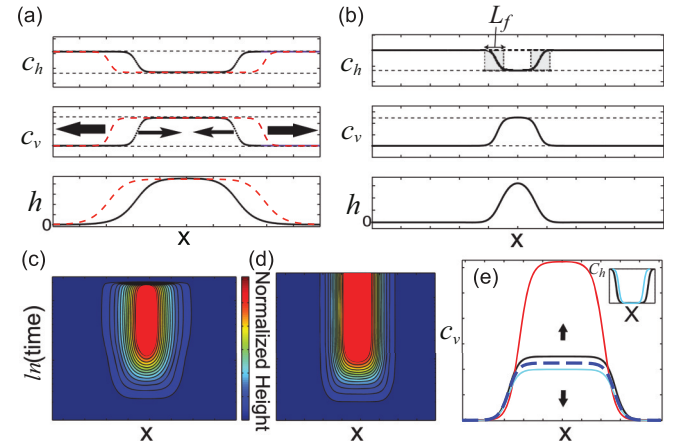


FIG. 4. (Color online) (a) Qualitative numerical representation of solutions to Eqs. (3) on periodic domains in the absence of actin-membrane coupling, i.e.,  $C_p = C'_p = 0$ . Black arrows depict the direction of front motion, i.e., either expansion or contraction with respect to the bottom uniform state, while the solid/dashed profiles correspond to two different times of the evolution and the horizontal dashed lines denote uniform solutions. For an expanding process  $t(\text{solid line}) < t(\text{dashed line})$ , the initial state ( $t = 0$ ) was a local perturbation located at the center of the domain. For a contracting process the times are  $t(\text{solid line}) > t(\text{dashed line})$  and the initial local perturbation was located at the domain ends. Asymptotically the system converges to a uniform state. (b) Numerical representation as in (a) but with  $C_p \neq 0$ . Here the system converges to a localized steady-state solution (LS). The edges of the LS are marked by the shaded box, and have a width  $L_f$ . (c), (d) Numerical space-time plots where contour levels correspond to normalized membrane height. In (c) the initial perturbation is below the threshold and eventually decays back to the stable uniform state, while a perturbation that is above threshold forms a stable LS (d). (e) Initial perturbation in  $c_v$  ( $c_h$  inset) for the cases shown in (c) and (d), bottom light and black lines, respectively. The threshold of the perturbation (dashed line) is characterized by both width and height. The bottom/top arrows indicate the respective temporal evolution direction in (c) and (d), while the top light line depicts the asymptotic LS profile in (d). Numerical calculations throughout this paper refer to periodic domains  $x \in [-50, 50]$  and time intervals  $t \in [0, 10^5]$  while (c)–(e) show a zoom into the space-time behavior within the peak region showed in (b). The parameters are given in Table I.

$c_h$  is therefore able to enter the borders of the protrusion region, pushing back the width of the bundled actin, and thereby restoring the LS to its steady-state width. The overall width of the LS increases with increasing strength of the coupling parameter above some critical value (bifurcation)  $C_{p,c}$ , while the width of the “fronts” [ $L_f$  in Fig. 4(a)] is largely independent.

The initial perturbation that evolves into the LS has to be above a threshold; otherwise it decays to the uniform steady state [Figs. 4(c) and 4(d)]. The initial conditions are of a local perturbation in the concentration fields of  $c_v, c_h$ , as shown in Fig. 4(e). This perturbation is characterized by both amplitude and width, and we found that both parameters control the threshold behavior. The threshold amplitude depends on the model parameters; for example it increases with the elastic stiffness of the membrane (through the membrane bending modulus or tension), as expected. Note that in the cell there are additional mechanisms that limit the lifetime of fully formed filopodia, such as capping proteins [47], which we do not explicitly describe in this model.

### C. Properties of localized states

Spatial localization means that once a single protrusion is formed, its shape is independent of the overall size of the system [19,48–51]. The LS connects the same uniform steady states at  $x \rightarrow \pm\infty$ , and approaches the second steady state at

the center of the LS. The decay of the fields to uniform states at infinity is exponential (Fig. 5).

The exponential decay to uniform states can be obtained by looking at the spatial properties of Eqs. (3), i.e., transformation to a set of ODEs where the prime stands for derivative with respect to a spatial coordinate. The equations together with  $S_{v2} = C'_p = 0$  (for simplicity) read

$$\begin{aligned} c'_v &= W_v, & c'_h &= W_h, & h' &= U, & U' &= U_{2h}, & U'_{2h} &= U_{3h}, \\ W'_v &= -c_v + c_v^3 + c_h, \\ W'_h &= -\frac{1}{D} [\varepsilon(-c_v - a_1 c_h + a_0) + C_p(W_h U_{2h} U \\ &\quad + c_h U_{2h}^2 + c_h U_{3h} U)], \\ U'_{3h} &= \frac{1}{\tilde{\kappa}} [c_v + S_{h1} U_{2h} - \tilde{\Omega} h + S_{h2}(W_h U + c_h U_{2h})]. \end{aligned} \quad (10)$$

The configuration of the spatial eigenvalues about the uniform state is important since localized states can form only at the intersection of two stable and two unstable manifolds [51,52]. To find the latter possibility, we linearize Eqs. (10) using

$$X \rightarrow X^* + \delta X + O(\delta X^2), \quad (11)$$

and obtain the following matrix:

$$\begin{pmatrix} \delta W'_v \\ \delta W'_h \\ \delta U'_{3h} \\ \delta c'_v \\ \delta c'_h \\ \delta h' \\ \delta U' \\ \delta U'_{2h} \end{pmatrix} = \begin{pmatrix} 0 & 0 & 0 & -1 + 3c_v^{*2} & 1 & 0 & 0 & 0 \\ 0 & 0 & 0 & \varepsilon D^{-1} & \varepsilon a_1 D^{-1} & 0 & 0 & 0 \\ 0 & 0 & 0 & \tilde{\kappa}^{-1} & 0 & -\tilde{\Omega} \tilde{\kappa}^{-1} & 0 & \tilde{\kappa}^{-1}(S_{h1} + S_{h2} c_h^*) \\ 1 & 0 & 0 & 0 & 0 & 0 & 0 & 0 \\ 0 & 1 & 0 & 0 & 0 & 0 & 0 & 0 \\ 0 & 0 & 0 & 0 & 0 & 0 & 1 & 0 \\ 0 & 0 & 0 & 0 & 0 & 0 & 0 & 1 \\ 0 & 0 & 1 & 0 & 0 & 0 & 0 & 0 \end{pmatrix} \begin{pmatrix} \delta W_v \\ \delta W_h \\ \delta U_{3h} \\ \delta c_v \\ \delta c_h \\ \delta h \\ \delta U \\ \delta U_{2h} \end{pmatrix}. \quad (12)$$

The approach to the uniform-state solutions (fixed points) is determined from the eigenvalues of the above matrix. We have numerically verified that the localized solution indeed approaches the uniform state exponentially  $X - X^* \propto \exp(\Theta x)$  ( $x \rightarrow \pm\infty$ ), where:

$$\Theta = \pm \sqrt{\frac{-D + a_1 \varepsilon + D c_v^{*2} \mp \sqrt{4D\varepsilon(1 + a_1 - a_1 c_v^{*2}) + [a_1 \varepsilon + D(-1 + c_v^{*2})]^2}}{2D}}, \quad (13a)$$

$$\Theta' = \pm \sqrt{\frac{S_{h1} + c_h^* S_{h2} \mp \sqrt{-4\tilde{\kappa} \tilde{\Omega} + (S_{h1} + c_h^* S_{h2})^2}}{2k}}, \quad (13b)$$

while all other eigenvalues are zero. The length scale  $\Theta^{-1}$  turns out to give a good measure for the width of the region over which the fields change at the sides of the localized solution.

In Fig. 5(a) we demonstrate the dependence of the overall width of the LS on the strength of the coupling parameter

$C_p$  between the membrane shape and the flux of branched network  $c_h$ . The fronts, i.e., the region over which the fields change their values from one uniform solution to the other, turn out to be independent of the coupling strength. Their width is very well approximated by the exponential form, with one of

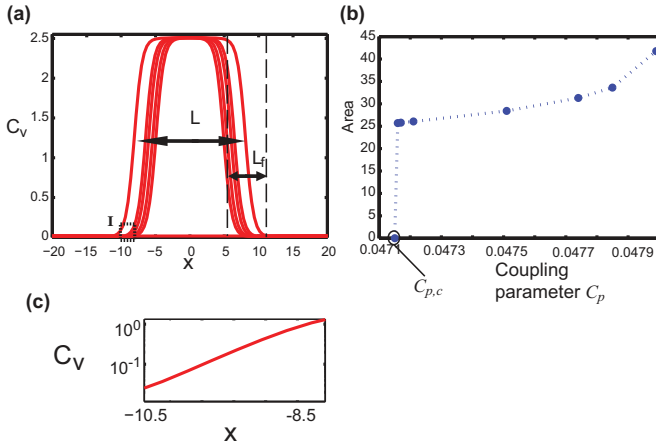


FIG. 5. (Color online) (a) Profiles of localized solutions for different coupling parameter  $C_p$  which are given in (b). We denote the full width of the LS by  $L$ , and the width of the “fronts” by  $L_f$ , where largest  $L$  corresponds to largest  $C_p$  on the top branch and vice versa. In (b) we show that the width (quantified by the overall area) increases with the coupling parameter, above a critical value  $C_{p,c}$ . (c) Plot of the region marked by I in (a), to show that the change in the concentration field in the profile follows an exponential behavior, which is well described by the linear analysis [Eqs. (13)].

the eigenvalues calculated in Eqs. (13). On the other hand, the width of LS increases with the coupling strength [Fig. 5(b)], as expected, since a shallower gradient in the membrane shape is able to produce a stronger expulsion current of  $c_h$  and stabilize the central region of the LS.

#### IV. EXPERIMENTS vs THEORY

Using detailed observations of the dynamics of filopodia formation in COS7 cells expressing GFP myosin-IIIa (in all the experiments described in this paper, we use a GFP-myosin-IIIa construct lacking the N-terminal kinase domain, which has enhanced motility and filopodia formation activity [28,43,53,54]), we found that myosin-IIIa induces filopodia formation and appears to localize to their tips in a continuous fashion while inactivated myosins are removed from the tips via actin retrograde flow [28]. Although we observed similar phenomena with myosins-XVa and -X, we chose to use data from our myosin-IIIa experiments since only this construct yielded a sufficient signal-to-noise ratio for quantitative analysis.

In Fig. 6, we show representative images of the distribution of GFP-labeled myosin-IIIa near the edge of a COS7 cell (see supporting videos S1, S2 [55]). We equate the local concentration of myosin-IIIa near the cell membrane with the local concentration of the bundled-actin elongators ( $c_v$ ) of our model. We show that the concentration of myosin-IIIa near the membrane fluctuates significantly, and only when the fluctuation locally reaches a threshold magnitude (both in amplitude and width) we find filopodia formation. This is similar to what has been observed for VASP [32,56], which is also involved in the elongation of filopodial actin bundles [57,58]. The source of these fluctuations is most likely dominated by active noise due to molecular motors and actin polymerization [59].

In Fig. 6, we define the overall projected area of the filopodia as the region where the myosin-IIIa intensity was

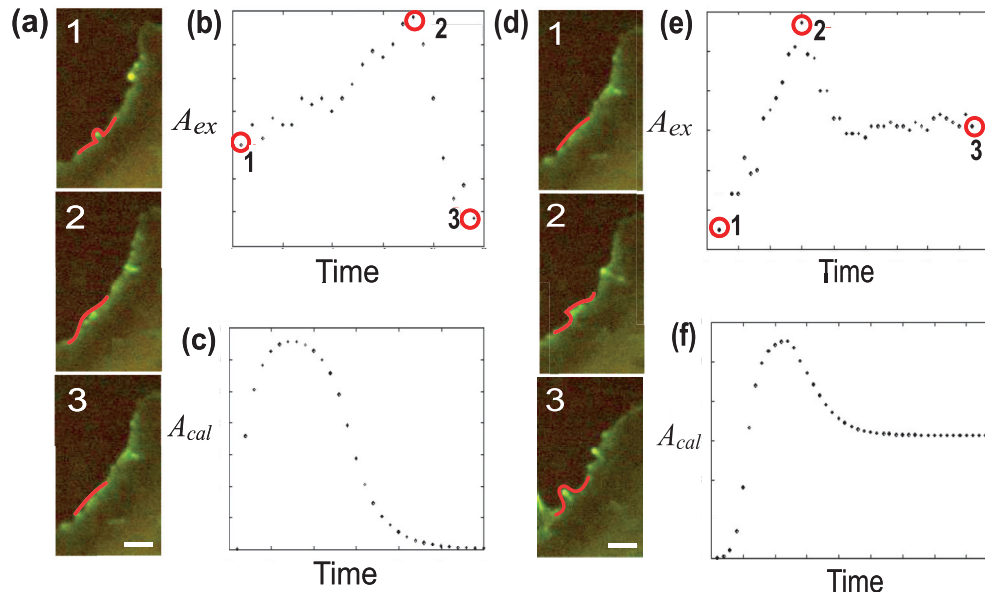


FIG. 6. (Color online) (a) Sample images extracted from the supporting video S1 [55], showing the dynamics of the intensity of fluorescently labeled myosin-IIIa near the cell membrane. These images illustrate how an extended perturbation in the protein concentration and membrane shape grows but eventually decays back to the uniform state (overall time 3 min). In (b) we plot the area ( $A_{ex}$ ) of the high-intensity region of myosin-IIIa near the membrane, extracted from the video (supporting videos S1, S2 [55]). This measurement represents approximately the projected area of the membrane protrusion, which we compare to the calculated area under the membrane ( $A_{cal}$ ) (c). (d)–(f) Similar to (a)–(d) for a region of the membrane where the perturbation was observed to grow and form a stable filopodia (overall time 5.2 min). Both in the experiment (e) and the theory (f) we observe an “overshoot” in the membrane area of the filopodia protrusion. Scale bars in (a) and (d) are  $2 \mu\text{m}$ .

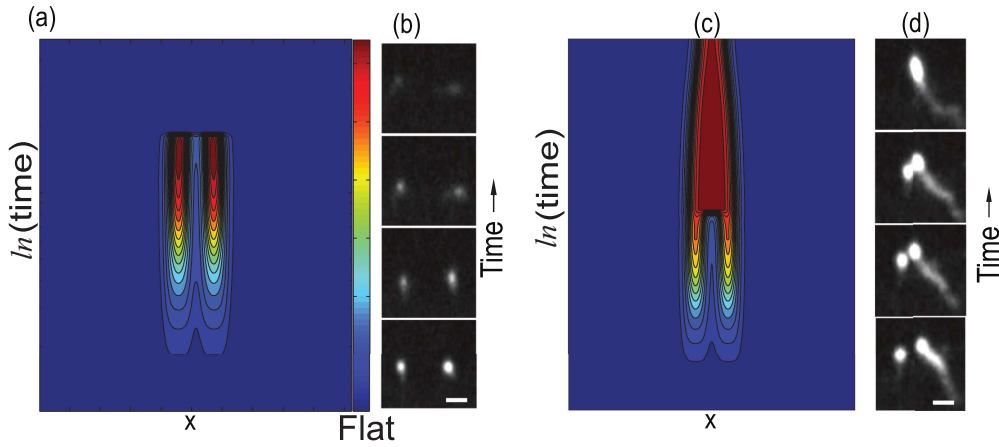


FIG. 7. (Color online) Interaction between perturbations. Space-time plots of the calculated membrane height evolution, for the case of two local perturbations in the concentration fields, where each perturbation alone is below threshold [as in Fig. 4(c)]. In (a) the two perturbations interact but are initially too far from each other and eventually decay to the uniform steady state. In (c) the same two perturbations are closer, and after coalescing they evolve to the LS. In (b) and (d) we show images from a movie (supporting video S2 [55]) where myosin-IIIa is fluorescently labeled, indicating the dynamics of bundled actin at the cell edge. In (b) two initial perturbations fail to coalesce and decay, while in (d) they are close enough to coalesce and form a filopodia. The overall time shown in (b) is 5.3 min, and in (d) 2.3 min. Scale bars in (b) and (d) are  $0.5 \mu\text{m}$ .

above some cutoff value [insets of Figs. 6(a) and 6(d)]. We found that below-threshold fluctuations are observed to grow and then decay without maturing into a stable filopodia (i), while in (ii) we show an example of a larger fluctuation that did reach the stable filopodia state. In the latter case we found an overshoot in the protrusion size before it converged into its final stable form. We have often observed that a fluctuation near the membrane can overcome the threshold value via coalescence with a neighboring fluctuation (see supporting videos S1,S2 [55]). Similar behavior is captured by the model, where we find that two initial perturbations that are close to each other interact and coalesce (Fig. 7). We chose the initial perturbations such that individually they are below the threshold, but when superimposed the combined perturbation is above threshold. The driving force in our model for the coalescence of neighboring protrusions is the minimization of the elastic energy of the membrane (similar to [16]). We find that when the two perturbations succeed to coalesce before they decay, indeed they are able to form a stable LS, as demonstrated in Fig. 7.

## V. CONCLUSIONS

We have shown that the mechanism for the filopodia formation can be understood from the coupling between biochemical reactions and mechanical deformations. The biochemical reactions describe mutually exclusive branched and bundled cortical actin [32,56], whereas the mechanical effects arise from membrane shape deformations. This model gives a realistic mechanism for the threshold phenomenon in filopodia formation, as well as capturing many qualitative features of observed dynamics during filopodia initiation.

One of the main predictions of our model is that protrusion formation is a dual threshold phenomenon: (i) The coupling strength between the branched network and the membrane  $C_p$  [Eq. (3d)] has to be above some minimal value  $C_{p,c}$  [Fig. 5(b)].

(ii) Even beyond the critical coupling the fluctuation needs to be above some threshold size (spatial extent and amplitude) for stable protrusion formation [Figs. 4(c)–4(e)]. These key conjectures were indicated by experiments. Our work also makes predictions about the parameters that control this threshold phenomenon, which remain to be systematically investigated by experiments and computations. An example of such a parameter that our model predicts to be important for protrusion formation is the membrane tension difference between the branched and bundled morphologies ( $\sigma'$  vs  $\sigma''$ ). Increasing this membrane tension difference increases the coupling parameter  $C_p$  and enables the initiation of filopodia. This conclusion is supported by the observation that enhanced binding of bundled actin and the membrane by ERM family proteins induces filopodia formation [35].

More generally, we introduce a theoretical approach to describe the coupling between a biochemical system that has multiple states and the biomechanical forces that arise from deformation of the elastic substrate. The developed RDE platform is therefore an important formulation which may facilitate the study of any phenomenon where a reaction-diffusion dynamics is coupled to mechanical forces and elastic deformations. Examples of which include stem cell differentiation [60], cardiac arrhythmia [9], and metastasis [61].

## ACKNOWLEDGMENT

This research is made possible in part by the historic generosity of the Harold Perlman Family.

## APPENDIX: THERMODYNAMIC APPROACH TO BISTABILITY IN CHEMICAL REACTIONS

We give here an example of a derivation of a system of chemical reactions that display bistability and have the general form of Eqs. (2a) and (2b) (without the membrane elasticity

part). We start with a Landau-Ginzburg form of the free energy which describes the adsorption of particles to a surface from the bulk (infinite) reservoir:

$$F[c_v] = \int dx \left[ -\frac{k_{\text{on}}^v}{2} c_v^2 + \frac{k_{\text{off}}}{4} c_v^4 \right]. \quad (\text{A1})$$

When both  $k_{\text{on}}^v$  and  $k_{\text{off}}$  are positive, we are in a regime of spontaneous adsorption to the surface. This is identical to the regime of coexistence between gas and condensed phases, where here the condensed phase describes the adsorbed

fraction on the surface (which is the membrane in Eqs. (2a) and (2b)). The rate of adsorption is then given by (the “dot” symbol stands for time derivative)

$$\dot{c}_v = -\Gamma \frac{\delta F[c_v]}{\delta c_v} = -\Gamma \Delta\mu, \quad (\text{A2})$$

where  $\Delta\mu$  is the total chemical potential difference between the bulk and the membrane-adsorbed proteins, and  $\Gamma$  is the kinetic coefficient. This form is identical to the dynamics of  $c_v$  in Eq. (2a).

- 
- [1] A. M. Turing, *Philos. Trans. R. Soc. London B* **237**, 37 (1952).  
 [2] M. C. Cross and P. C. Hohenberg, *Rev. Mod. Phys.* **65**, 851 (1993).  
 [3] J. D. Murray, *Mathematical Biology*, Vol. 2 (Springer, 2002).  
 [4] J. Lewis, *Science* **322**, 399 (2008).  
 [5] T. Duke and F. Julicher, *Phys. Rev. Lett.* **90**, 158101 (2003).  
 [6] A. Garfinkel, Y. Tintut, D. Petrasek, K. Boström, and L. L. Demer, *Proc. Natl. Acad. Sci. USA* **101**, 9247 (2004).  
 [7] S. Sick, S. Reinker, J. Timmer, and T. Schlake, *Science* **314**, 1447 (2006).  
 [8] J. Howard, S. W. Grill, and J. S. Bois, *Nat. Rev. Mol. Cell Biol.* **12**, 392 (2011).  
 [9] A. V. Panfilov, R. H. Keldermann, and M. P. Nash, *Proc. Natl. Acad. Sci. USA* **104**, 7922 (2007).  
 [10] H. M. Eilken and R. H. Adams, *Curr. Opin. Cell Biol.* **22**, 617 (2010).  
 [11] S. L. Gupton and F. B. Gertler, *Sci. STKE* **2007**, re5 (2007).  
 [12] P. K. Mattila and P. Lappalainen, *Rev. Mol. Cell Biol.* **9**, 446 (2008).  
 [13] A. Mogilner and B. Rubinstein, *Biophys. J.* **89**, 782 (2005).  
 [14] Y. Lan and G. A. Papoian, *Biophys. J.* **94**, 3839 (2008).  
 [15] P. I. Zhuravlev, B. S. Der, and G. A. Papoian, *Biophys. J.* **98**, 1439 (2010).  
 [16] E. Atilgan, D. Wirtz, and S. X. Sun, *Biophys. J.* **90**, 65 (2006).  
 [17] F. Vaggi, A. Disanza, F. Milanese, P. P. Di Fiore, E. Menna, M. Matteoli, N. S. Gov, G. Scita, and A. Ciliberto, *PLoS Comput. Biol.* **7**, e1002088 (2011).  
 [18] C. Yang and T. Svitkina, *Cell Adh. Migr.* **5**, 402 (2011).  
 [19] E. Knobloch, *Nonlinearity* **21**, T45 (2008).  
 [20] N. S. Gov and A. Gopinathan, *Biophys. J.* **90**, 454 (2006).  
 [21] A. Veksler and N. S. Gov, *Biophys. J.* **93**, 3798 (2007).  
 [22] S. Whitelam, T. Bretschneider, and N. J. Burroughs, *Phys. Rev. Lett.* **102**, 198103 (2009).  
 [23] I. Hecht, D. A. Kessler, and H. Levine, *Phys. Rev. Lett.* **104**, 158301 (2010).  
 [24] A. Disanza, S. Mantoani, M. Hertzog, S. Gerboth, E. Frittoli, A. Steffen, K. Berhoerster, H. J. Kreienkamp, F. Milanese, P. P. Di Fiore *et al.* *Nat. Cell Biol.* **8**, 1337 (2006).  
 [25] D. Breitsprecher, A. K. Kiesewetter, J. Linkner, C. Urbanke, G. P. Resch, J. V. Small, and J. Faix, *EMBO J.* **27**, 2943 (2008).  
 [26] S. D. Hansen and R. D. Mullins, *J. Cell. Biol.* **191**, 571 (2010).  
 [27] S. Khurana and S. P. George, *Cell Adh. Migr.* **5**, 409 (2011).  
 [28] F. T. Salles, R. C. Merritt, U. Manor, G. W. Dougherty, A. D. Sousa, J. E. Moore, C. M. Yengo, A. C. Dose, and B. Kachar, *Nat. Cell Biol.* **11**, 443 (2009).  
 [29] T. M. Svitkina, E. A. Bulanova, O. Y. Chaga, D. M. Vignjevic, S. Kojima, J. M. Vasiliev, and G. G. Borisy, *J. Cell. Biol.* **160**, 409 (2003).  
 [30] C. Yang, L. Czech, S. Gerboth, S. Kojima, G. Scita, and T. Svitkina, *PLoS Biol.* **5**, e317 (2007).  
 [31] S. A. Johnston, J. P. Bramble, C. L. Yeung, P. M. Mendes, and L. M. Machesky, *BMC Cell Biology* **9**, 65 (2008).  
 [32] G. T. Charras, M. Coughlin, T. J. Mitchison, and L. Mahadevan, *Biophys. J.* **94**, 1836 (2008).  
 [33] J. Dai and M. P. Sheetz, *Biophys. J.* **77**, 3363 (1999).  
 [34] N. Gov and S. A. Safran, *Phys. Rev. E* **69**, 011101 (2004).  
 [35] A. Bretscher, K. Edwards, and R. G. Fehon, *Rev. Mol. Cell Biol.* **3**, 586 (2002).  
 [36] W. Helfrich, *Z. Naturforsch. C* **28**, 693 (1973).  
 [37] N. Offenhauser, A. Borgonovo, A. Disanza, P. Romano, I. Ponzanelli, G. Iannolo, P. P. Di Fiore, and G. Scita, *Mol. Biol. Cell* **15**, 91 (2004).  
 [38] M. Hertzog, F. Milanese, L. Hazelwood, A. Disanza, H. J. Liu, E. Perlade, M. G. Malabarba, S. Pasqualato, A. Maiolica, S. Confalonieri *et al.* *PLoS Biol.* **8**, e1000387 (2010).  
 [39] H. Nakagawa, H. Miki, M. Ito, K. Ohashi, T. Takenawa, and S. Miyamoto, *J. Cell Sci.* **114**, 1555 (2001).  
 [40] H. Tokuo, K. Mabuchi, and M. Ikebe, *J. Cell. Biol.* **179**, 229 (2007).  
 [41] M. L. Kerber and R. E. Cheney, *J. Cell Sci.* **124**, 3733 (2011).  
 [42] J. Lin-Jones, E. Parker, M. Wu, A. Dose, and B. Burnside, *J. Cell Sci.* **117**, 5825 (2004).  
 [43] O. A. Quintero, J. E. Moore, W. C. Unrath, U. Manor, F. T. Salles, M. Grati, B. Kachar, C. M. Yengo *et al.*, *J. Biol. Chem.* **285**, 35770 (2010).  
 [44] M. L. Kerber, D. T. Jacobs, L. Campagnola, B. D. Dunn, T. Yin, A. D. Sousa, O. A. Quintero, and R. E. Cheney, *Curr. Biol.* **19**, 967 (2009).  
 [45] J. Nagumo, S. Arimoto, and S. Yoshizawa, *Proc. IRE* **50**, 2061 (1962).  
 [46] R. FitzHugh, *Biophys. J.* **1**, 445 (1961).  
 [47] P. I. Zhuravlev and G. A. Papoian, *Proc. Natl. Acad. Sci. USA* **106**, 11570 (2009).  
 [48] A. Yochelis and A. Garfinkel, *Phys. Rev. E* **77**, 035204 (2008).  
 [49] A. Yochelis, Y. Tintut, L. L. Demer, and A. Garfinkel, *New J. Phys.* **10**, 055002 (2008).  
 [50] J. Burke, A. Yochelis, and E. Knobloch, *SIAM J. Appl. Dyn. Syst.* **7**, 651 (2008).

- [51] J. Burke and E. Knobloch, *Phys. Rev. E* **73**, 056211 (2006).
- [52] A. R. Champneys, *Physica D* **112**, 158 (1998).
- [53] M. E. Schneider, A. C. Dose, F. T. Salles, W. Chang, F. L. Erickson, B. Burnside, and B. Kachar, *J. Neurosci.* **26**, 10243 (2006).
- [54] R. C. Merritt, U. Manor, F. T. Salles, M. Grati, A. C. Dose, W. C. Unrath, O. A. Quintero, C. M. Yengo, and B. Kachar, *Curr. Biol.* **22**, 320 (2012).
- [55] See Supplemental Material at <http://link.aps.org/supplemental/10.1103/PhysRevE.88.022718> for the experimental movies showing the dynamics of the filopodia formation and bundled actin accumulation through labeled myosin-IIIa.
- [56] D. Vignjevic, D. Yarar, M. D. Welch, J. Peloquin, T. Svitkina, and G. G. Borisy, *J. Cell. Biol.* **160**, 951 (2003).
- [57] C. Lebrand, E. W. Dent, G. A. Strasser, L. M. Lanier, M. Krause, T. M. Svitkina, G. G. Borisy, and F. B. Gertler, *Neuron* **42**, 37 (2004).
- [58] K. Lee, J. L. Gallop, K. Rambani, and M. W. Kirschner, *Science* **329**, 1341 (2010).
- [59] D. Mizuno, C. Tardin, C. F. Schmidt, and F. C. MacKintosh, *Science* **315**, 370 (2007).
- [60] A. J. Engler, S. Sen, H. L. Sweeney, and D. E. Discher, *Cell* **126**, 677 (2006).
- [61] A. Pathak and S. Kumar, *Integr. Biol.* **3**, 267 (2011).